Available on CMS information server

CMS DP -2024/004

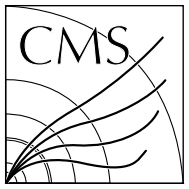

The Compact Muon Solenoid Experiment

CMS Performance Note

Mailing address: CMS CERN, CH-1211 GENEVA 23, Switzerland

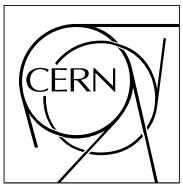

06 December 2023

XY-factorization correction for luminosity calibration using off-axis scans for 2022 pp data at 13.6 TeV

CMS Collaboration

Abstract

This note describes the results of the XY-factorization analysis of the CMS 2022 proton-proton luminosity calibration at 13.6 TeV center-of-mass energy using on-axis Van-der-Meer and off-axis diagonal or offset scans.

XY-factorization correction for luminosity calibration using off-axis scans for 2022 pp data at 13.6 TeV

CMS Collaboration

contact:
cms-pog-conveners-lum@cern.ch

Abstract and introduction

The luminosity measurement of the CMS experiment is calibrated in special LHC fills where the beams are separated in various steps in the transverse direction as described in *Eur. Phys. J. C 81 (2021) 800*.

The van der Meer (vdM) method is based on the assumption that the beam particle density function is factorizable in the transverse directions $\varrho(x,y)=\varrho_x(x)\cdot\varrho_y(y)$, which leads to a bias of the calibration constant, the visible cross-section of a luminometer, is proportional to the integral of the beam overlap function $\sigma_{vis} \propto \iint (\varrho_1*\varrho_2)(x,y)dxdy \cong 2\pi\cdot\max(\varrho_1*\varrho_2)\cdot\Sigma_x\Sigma_y$, with $\varrho_{1/2}$ being the beam particle density of beam 1/2 and $\Sigma_{x/y}$ being the beam overlap width in the x/y direction.

The CMS experiment employed several methods to assess the size of this non-factorization bias and to derive a correction on the visible cross section. The results presented here for the 2022 pp data taking at 13.6 TeV belong to the offset-scan (CMS-PAS-LUM-18-002) and diagonal-scan (CMS-PAS-LUM-18-001) analyses, both of which apply 2D fits to the beam overlap shapes sampled by the traditional on-axis scans (vdM) and the off-axis: offset (offs), diagonal (diag) or mini-diagonal (mini) scans to derive the correction. Seven on-axis scan - off-axis scan pairs are used, in time order: vdM2 + diag, diag + vdM3, vdM3 + mini1, vdM3 + offs, mini1 + vdM4, offs + vdM4, vdM4 + mini2 (see also next slide for naming convention).

The vdM data in 1D (along the X or Y axis) are fitted by a double Gaussian function. The following eight 2D fit functions in the X - Y plane are used to asses the factorization (see in details on the next slide): single Gaussian (SG), super Gaussian (supG), q-Gaussian (qG), polynomial Gaussian (polyG) where the constant of the Gaussian function is replaced by a symmetric 4th order polynomial, and double Gaussian with a common mean (DG). Various constraints are also applied on the double Gaussian parameters to improve their convergence properties and study their most important features: the axes of the Gaussians must have the same orientation (DG_AxisFixed); in addition, their width ratios must be also equal (DG_TiltFixed). Furthermore, the generic double Gaussian fit can also be performed in two steps: first the correlation parameters set to zero and the released (DG_RhoReleased).

The rate data of the five luminometers are used: the beam condition monitor “fast” read out by VME electronics (BCM1F) or uTCA electronics which uses digital signal processing to improve the performance (BCM1FUTCA), the pixel luminosity telescope (PLT), and the hadron forward calorimeter using either a tower counting (HFOC) or a transverse energy sum (HFET) method.

There were 144 colliding bunch pairs in CMS during the pp LHC fill 8381. Each identified by a unique bunch crossing identification (BCID) between 0 to 3563.

In total more than 350k measurements for 7 (scan-scan pairs) x 5 (luminometers) x 8 (2-dimensional shape models) x 144 (BCIDs) x 9 (orbit drift variations) are used to derive the factorization correction, which should only depend on the bunch shapes, and thus the BCID and the scan-scan pair due to the shape evolution in time.

Glossary of 2D Fit Functions Used to Assess the Factorization I.

All functions are defined in the *X-Y* plane (having *x* and *y* as variables).

General shorthand notation: $r^2 = \frac{\left(\frac{x-\mu_x}{\sigma_x}\right)^2 + \left(\frac{y-\mu_y}{\sigma_y}\right)^2 - 2\varrho\frac{x-\mu_x}{\sigma_x}\frac{y-\mu_y}{\sigma_y}}{1-\varrho^2}$.

- single Gaussian (**SG**):

$$f_{\mathrm{SG}}(x,y;V,\mu_x,\mu_y,\sigma_x,\sigma_y,\varrho) = \frac{V}{2\pi\sigma_x\sigma_y\sqrt{1-\varrho^2}}\exp\left(-\frac{r^2}{2}\right)$$

- super Gaussian (**supG**):

$$f_{\mathrm{supG}}(x,y) = \frac{V}{N}\exp\left(-\frac{r^{2p}}{2}\right)$$

  - Normalization here:

$$N = 2\pi\sigma_x\sigma_y\sqrt{1-\varrho^2}\cdot\frac{\Gamma(1/p)}{p}2^{1/p}$$

Glossary of 2D Fit Functions Used to Assess the Factorization II.

- q-Gaussian (**qG**):

$$f_{\mathrm{qG}}(x,y) = \frac{V}{C(q)\cdot\sigma_x\sigma_y\sqrt{1-\varrho^2}}\cdot e_q\left(-\frac{r^2}{(4-2q)}\right)$$

  - positivity marked as: $[x]_+$
  - functions for qG:

$$e_q(x) = \left[1+(1-q)x\right]_+^{\frac{1}{1-q}}$$

$$C(q) = \begin{cases} \frac{4-2q}{1-q}\pi\frac{\Gamma\left(\frac{2-q}{1-q}\right)}{\Gamma\left(\frac{2-q}{1-q}+1\right)} & q<1 \\ \frac{4-2q}{q-1}\pi\frac{\Gamma\left(\frac{1}{q-1}-1\right)}{\Gamma\left(\frac{1}{q-1}\right)} & \text{otherwise} \end{cases}$$

- polynomial Gaussian (**polyG**): constant of Gaussian function replaced by symmetric 4th order polynomial

$$f_{\mathrm{polyG}}(x,y;V,\mu_x,\mu_y,\sigma_x,\sigma_y,\varrho,a_2,\bar{a}_4) = \frac{V}{N}(1+a_2r^2+a_4r^4)\cdot\exp\left(-\frac{r^2}{2}\right)$$

  - For positivity: $\bar{a}_4 > 0$, where:
  - Normalization here:

$$a_4 = \begin{cases} \bar{a}_4 & \text{if } a_2 > 0, \\ \bar{a}_4 + a_2^2/4 & \text{otherwise.} \end{cases}$$

$$N = 2\pi\sigma_x\sigma_y\sqrt{1-\varrho^2}\cdot(1+2a_2+8a_4)$$

Glossary of 2D Fit Functions Used to Assess the Factorization III.

- double Gaussian (**DG**):
  - With common mean

$$f_{\mathrm{DG}}(x,y) = V \cdot \Big(v_R \cdot f_{\mathrm{SG}}\Big(x,y;1,\mu_x,\mu_y,\sigma_x^{(1)},\sigma_y^{(1)},\varrho^{(1)}\Big) + (1-v_R)\cdot f_{\mathrm{SG}}\Big(x,y;1,\mu_x,\mu_y,\sigma_x^{(2)},\sigma_y^{(2)},\varrho^{(2)}\Big)\Big)$$

  - **DG_TiltFixed:**
    - Axes of the Gaussians must have the same orientation

$$f_{\mathrm{DGv2}}(x,y) = V \cdot \Big(v_R \cdot f_{\mathrm{SG}}\Big(x,y;1,\mu_x,\mu_y,\sigma_x^{(1)},\sigma_y^{(1)},\varrho+\mathrm{d}\varrho\Big) + (1-v_R)\cdot f_{\mathrm{SG}}\Big(x,y;1,\mu_x,\mu_y,\sigma_x^{(2)},\sigma_y^{(2)},\varrho-\mathrm{d}\varrho\Big)\Big)$$

    - Where the sigmas are correspondingly the following:

$$\begin{aligned}
\sigma_x^{(1)} &= \sigma_x\sqrt{s_R}\sqrt{s_A},\\
\sigma_y^{(1)} &= \sigma_y\sqrt{s_R}/\sqrt{s_A},\\
\sigma_x^{(2)} &= \sigma_x/\sqrt{s_R}/\sqrt{s_A},\\
\sigma_y^{(2)} &= \sigma_y/\sqrt{s_R}\sqrt{s_A}.
\end{aligned}$$

Glossary of 2D Fit Functions Used to Assess the Factorization IV.

- **DG_AxisFixed:**
  - Rotation of components are set to be identical

$$f_{\mathrm{DGv3}}(x,y) = V \cdot \Big(v_R \cdot f_{\mathrm{SG}}^{(\alpha)}\left(x,y;1,\mu_x,\mu_y,\sigma_x^{(1)},\sigma_y^{(1)},\alpha+\mathrm{d}\alpha\right) + (1-v_R)\cdot f_{\mathrm{SG}}^{(\alpha)}\left(x,y;1,\mu_x,\mu_y,\sigma_x^{(2)},\sigma_y^{(2)},\alpha-\mathrm{d}\alpha\right)\Big)$$

  - Using reparametrized SG:

$$f_{\mathrm{SG}}^{(\alpha)}(x,y;V,\mu_x,\mu_y,\sigma_x,\sigma_y,\alpha) = \frac{V}{2\pi\sigma_x\sigma_y\sqrt{1-\varrho^2}} \cdot \exp\left(-\frac{r_\alpha^2}{2}\right)$$

    - Where with a 2x2 rotation matrix $R(\alpha)$:

$$r_\alpha^2 = \begin{pmatrix} x-\mu_x \\ y-\mu_y \end{pmatrix}^T R(-\alpha) \begin{pmatrix} \sigma_x^{-2} & 0 \\ 0 & \sigma_x^{-2} \end{pmatrix} R(\alpha) \begin{pmatrix} x-\mu_x \\ y-\mu_y \end{pmatrix}$$

2022 pp VdM scan program and data labeling

Not a CMS plot,
for illustration only

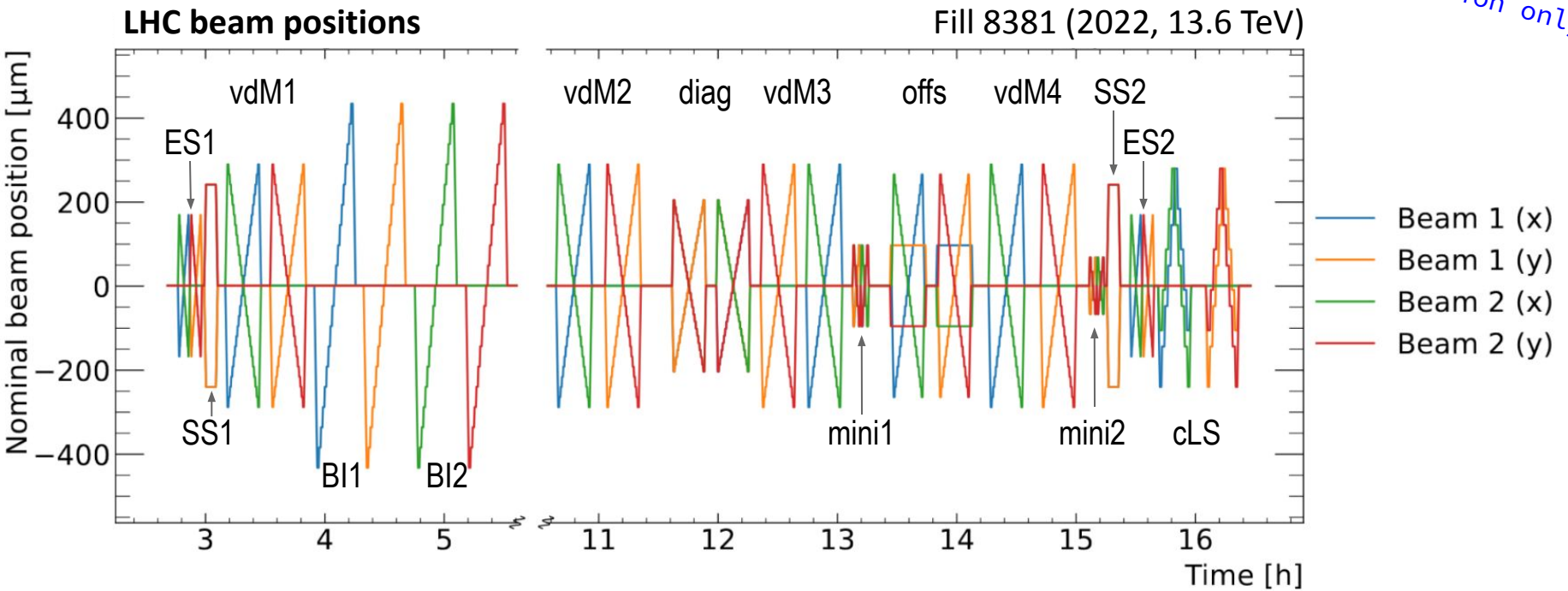

Figure 1: Nominal transverse beam positions (defined by the currents of the LHC dipole corrector magnets) as a function of time during LHC fill 8381. The labels of the various scan pairs are also given. Each scan pair contains two scans orthogonal to each other (e.g., horizontal vdM2X and vertical vdM2Y). Abbreviations: emittance scan (ES), super-separation (SS), van der Meer scan (vdM), beam imaging scan (BI), diagonal scan (diag), mini-diagonal scan (mini), offset scan (offs), constant length scale scan (cLS). When several scans of the same type are performed, a number also follows the abbreviations to create unique labels. During the time gap between 5:36 and 10:36 CMS was taking head-on data.

2022 vdM & Off-Axis Scans

Not a CMS plot,
for illustration only

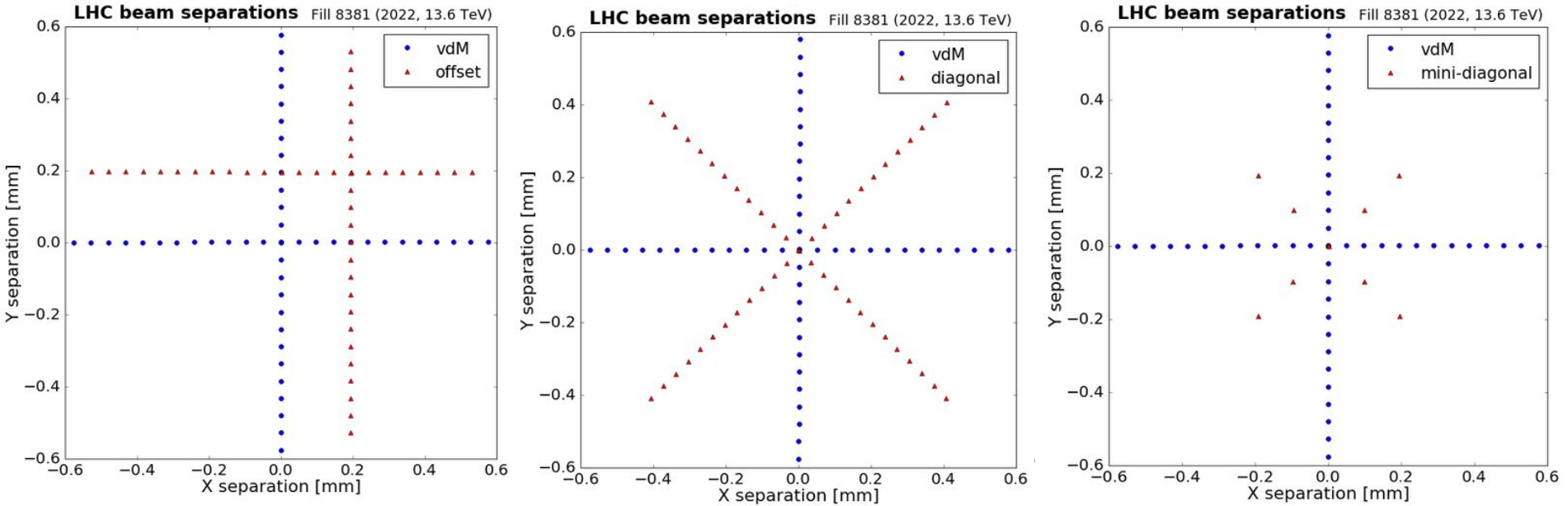

Figure 2: Nominal transverse beam separations (defined by the currents of the LHC dipole corrector magnets) in X and Y directions during scans to illustrate the different scan types performed in 2022. The separation points (the distances by which the beams are separated) for vdM scans in X and Y directions are shown in blue, while for the off-axis scan points are marked in red. The latter can belong to (left) offset, (middle) diagonal or (right) mini-diagonal scans.

Input Data - vdM & Off-Axis Scans

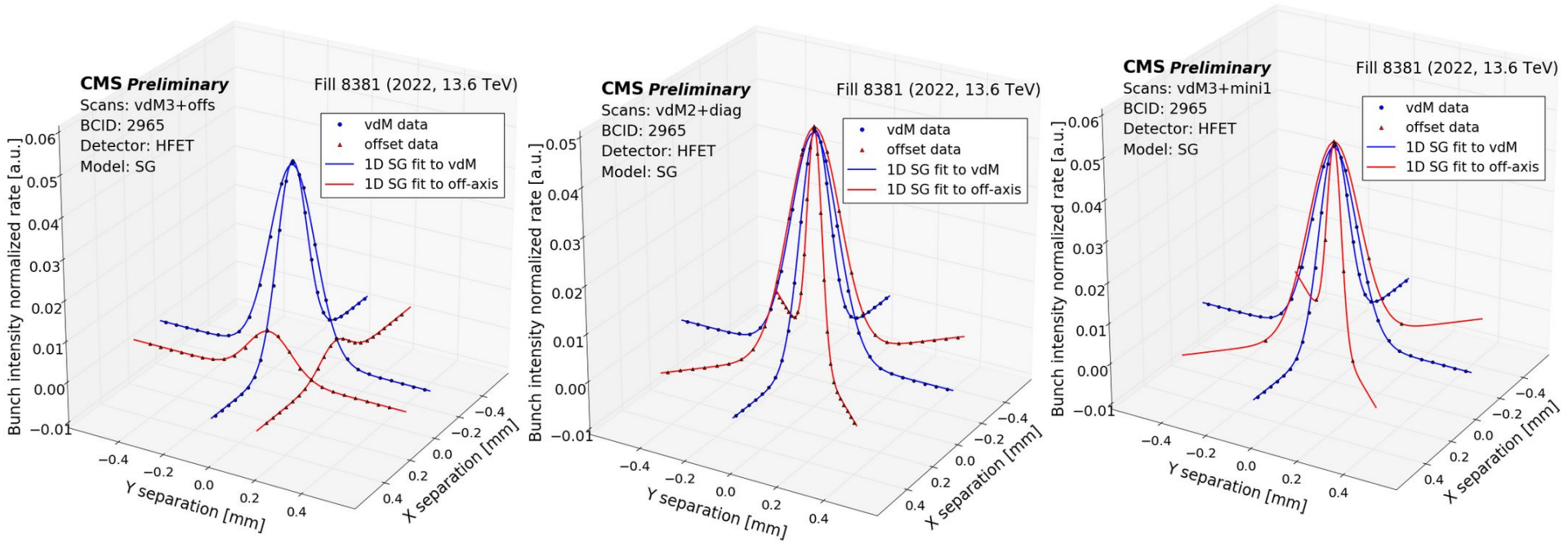

Figure 3: Visualization of the HFET data at the scan points connected by 1D single Gaussian fits in on-axis vdM (blue) and off-axis (red) scans for (left) offset, (middle) diagonal and (right) mini-diagonal scan pairs. A simultaneous 2D fit is performed in each case to the luminometer data to study the factorization property of the beam overlap shape sampled by the on- and off-axis scan pairs.

Beam overlap width ratios

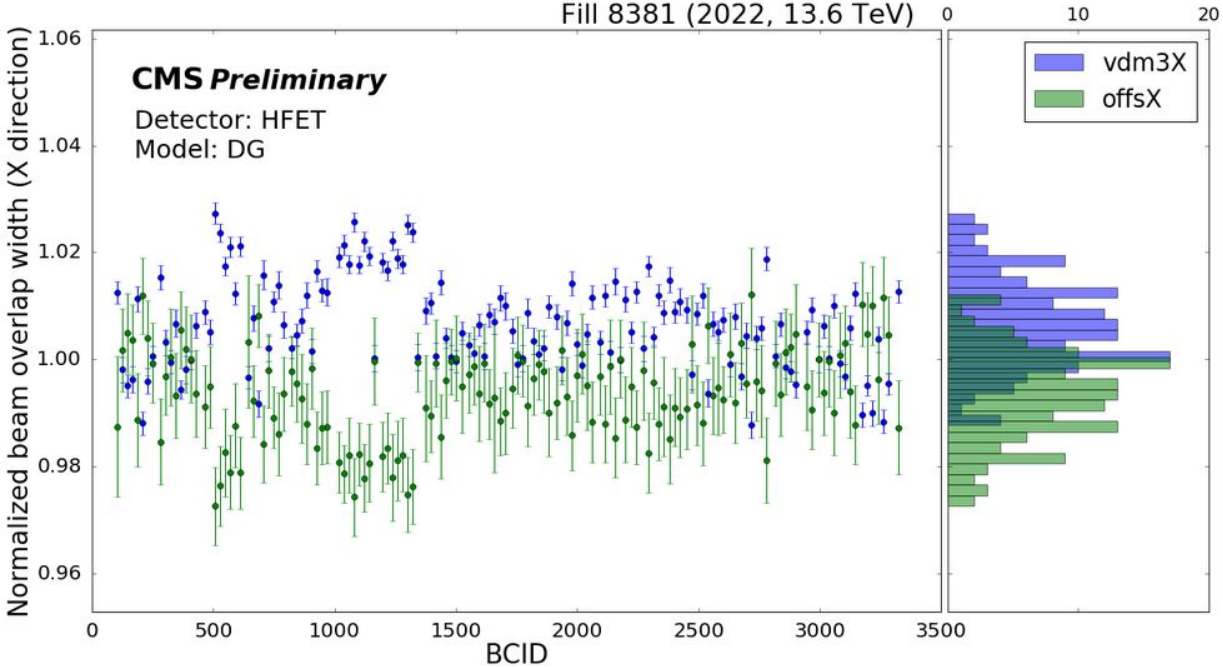

Figure 4: Dependence of the width ratio on the bunch crossing identification (BCID), i.e. the position of the colliding bunch pair in the LHC orbit: the measured beam overlap width in the X direction from the third vdM (blue) and the subsequent offset (green) scan curves divided by the average of the two values. To extract the widths, the HFET data are fitted in 1D using a double Gaussian model.

Additional orbit drift correction

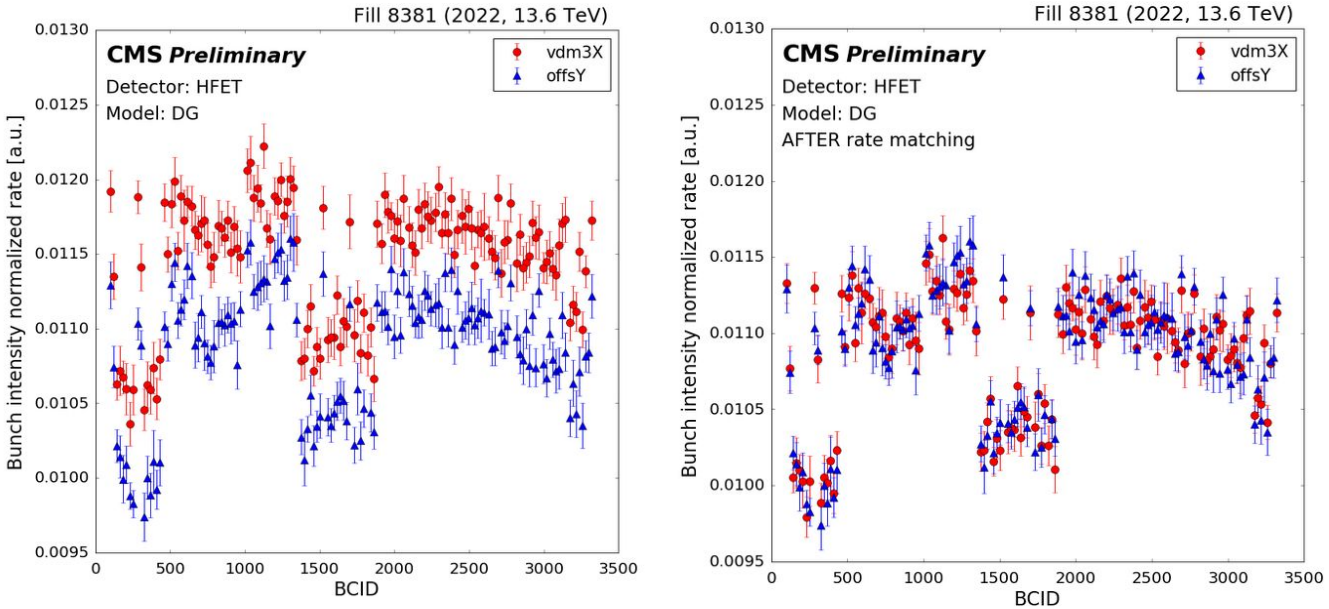

Figure 5: Bunch intensity normalized rates as a function of the bunch crossing identification (BCID) for the HFET counting method for the separation point where the third vdM scan X direction (vdM3X) and the offset scan Y direction (offsY) patterns meet. For offset scans, due to the fast change of the rate with separation, even a small change in the separation can have a significant effect. Therefore, an additional correction is used on the offset scan data to ensure that the rates match at the “common” scan point. This functions as an additional orbit-drift correction in the non-scanning direction of the offset scan. A linear orbit drift correction is applied on the input data based on the beam position measurements by DOROS (Diode ORbit and OScillation) system before this step. The left plot shows the rates in the crossing point before, while the right plot after the additional orbit drift obtained from the rate matching. The measurement can only be performed in the non-scanning direction, however its result is also used as a ± variation to estimate the possible effect of an unknown orbit drift.

Additional orbit drift correction II.

Figure 6: Observed beam separation in the non-scanning direction of the offset scan in the scan point where the vdM and offset scan trajectories cross, computed from the rate matching procedure. As an example, the case with the largest additional orbit shift is shown which is realized for the comparison of the measurements of the third vdM scan in Y direction (vdM3Y) and of the offset scan in the X direction (offsx). The results using the data of different luminometers agree with an RMS of 0.1 µm. The nominal separations are defined by the currents of the LHC dipole corrector magnets. The so-called linear orbit drifts (OD) are calculated from the DOROS beam position monitor data taken head-on before and after the scans. The uncertainty on the observed separation is calculated from the RMS of the results over the five luminometers.

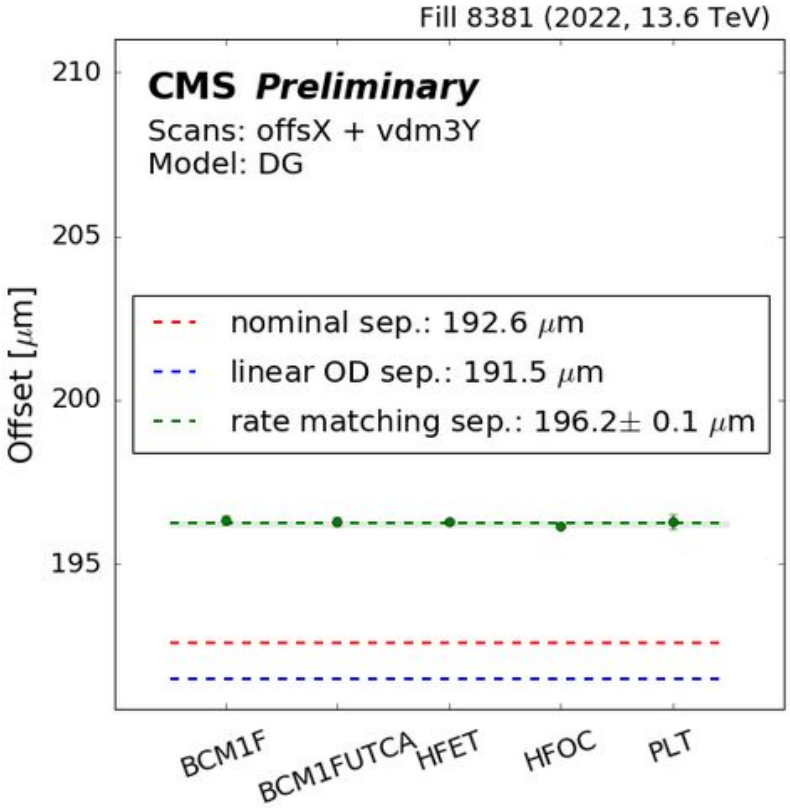

2D Fit: vdM scan - offset scan pair

Figure 7: Comparison of the 1D (X or Y) vdM fit results using double Gaussian functions (dashed green lines) with the 2D (X - Y) fit result using a polynomial Gaussian shape (rainbow contours to illustrate the shape and orange lines for the slices). The scan points in the X separation - Y separation plane are indicated (blue dots). The HFET data is shown in a vdM scan + offset scan pair. The rates are normalized with different factors for better visibility for the vdM and offset scan slices.

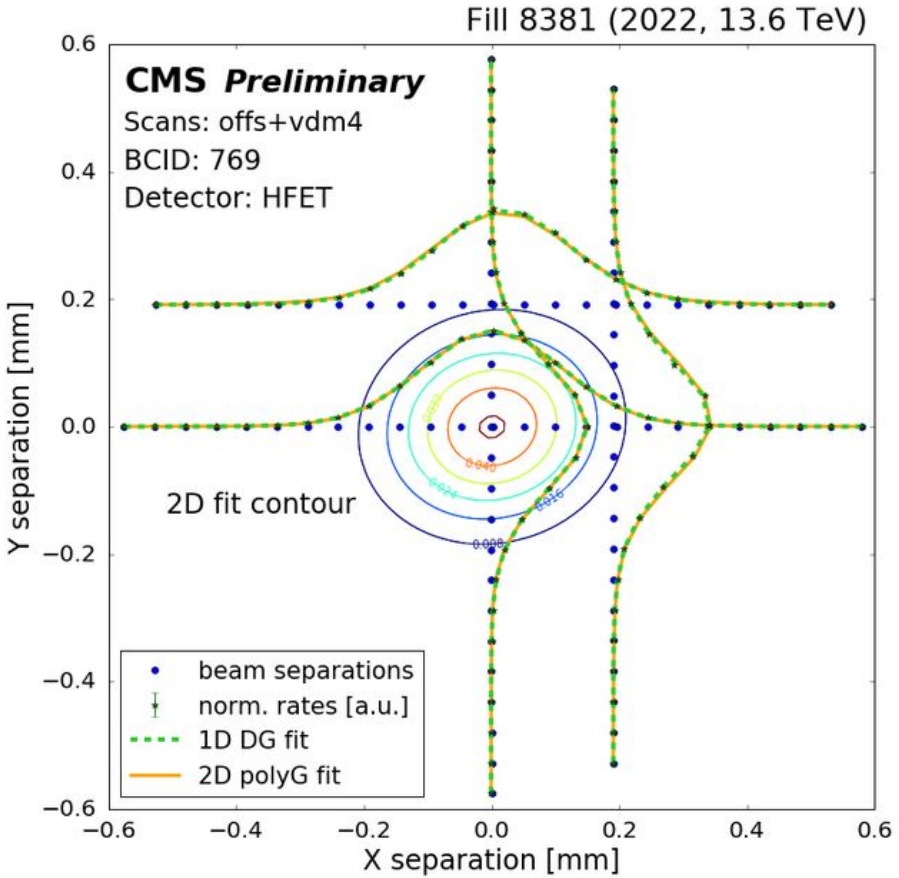

Correction vs Shape Parameter

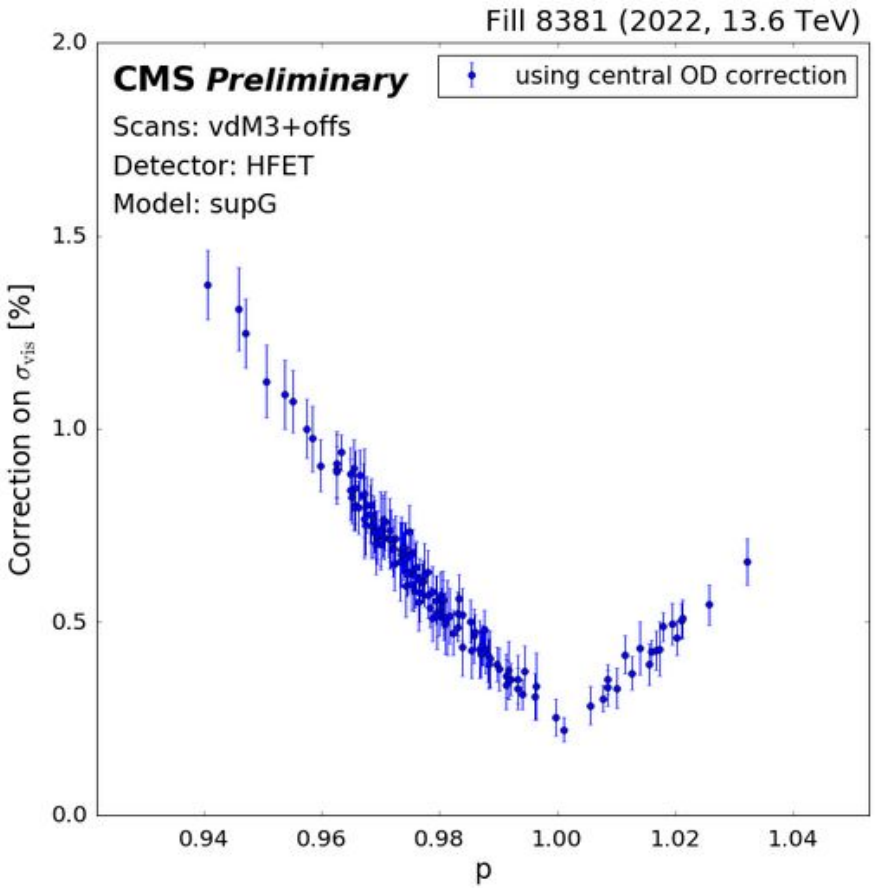

Figure 8: Dependence of the correction on the visible cross section (σ_{vis}, the detector and counting method dependent calibration constant) on the characteristic shape parameter p of the super Gaussian model, plotting the results for all colliding bunch pairs with good fit results using the HFET data for the third vdM scan - offset scan pair, and the central value for the additional orbit drift. The *p* parameter controls the sharpness of the peak. Values of $p>1$ imply a peak that is flatter than a Gaussian distribution.

The parametrization used for the super Gaussian function:

$$f(x,y;V,\mu_x,\mu_y,\sigma_x,\sigma_y,\varrho,p) = \frac{V}{N}\exp\left(-\frac{r^{2p}}{2}\right)$$

$$N = 2\pi\sigma_x\sigma_y\sqrt{1-\varrho^2}\cdot\frac{\Gamma(1/p)}{p}2^{1/p} \qquad r^2 = \frac{\left(\frac{x-\mu_x}{\sigma_x}\right)^2+\left(\frac{y-\mu_y}{\sigma_y}\right)^2-2\varrho\frac{x-\mu_x}{\sigma_x}\frac{y-\mu_y}{\sigma_y}}{1-\varrho^2}$$

Corrections vs BCID (an example with HFET data)

Figure 9: An example of the derived XY factorization corrections as a function of the bunch crossing identification (BCID). In this example, the HFET data is fitted with a 2D polynomial Gaussian model to derive the correction on the visible cross section (σ_{vis}) using the diagonal scan and the closes (third) vdM scan following it. The central value for the orbit drift correction is applied. The uncertainties are statistical only. The average correction and the RMS over all BCIDs with good fit results are also indicated.

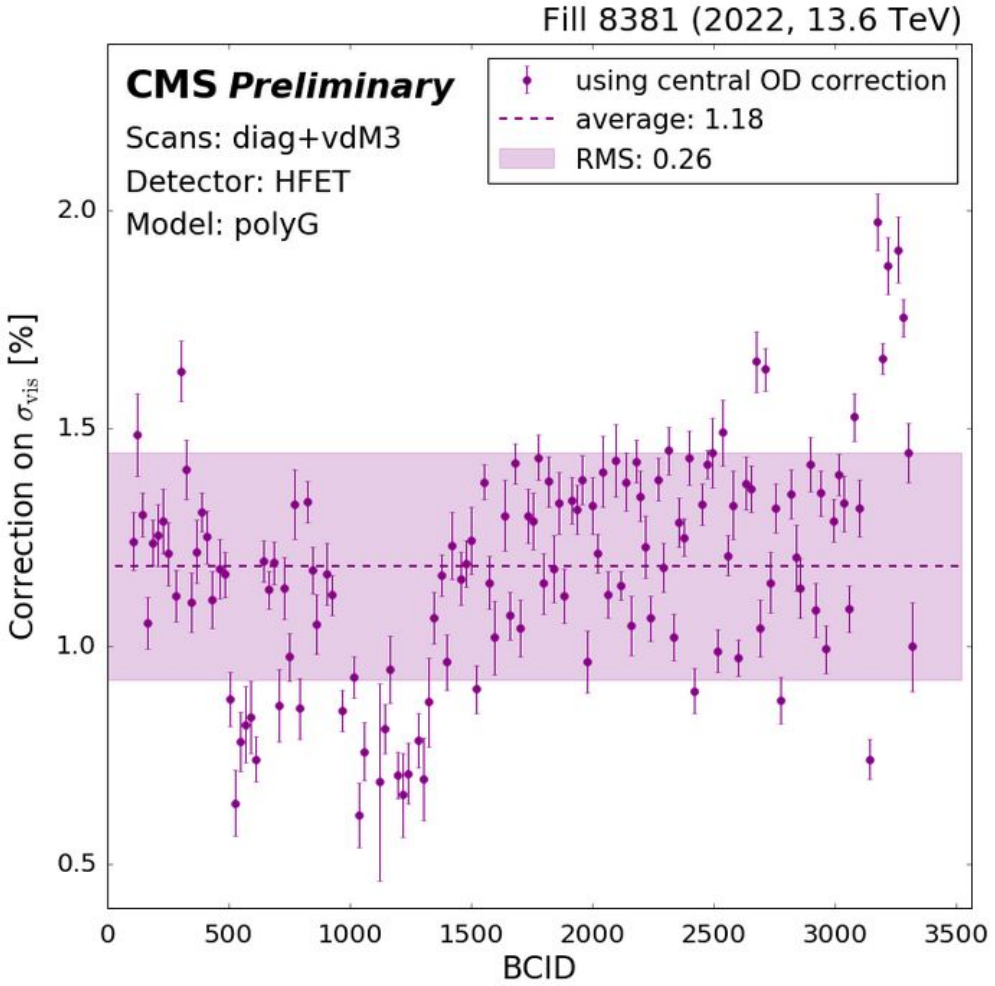

Corrections with Different Luminometers

Figure 10: Correlation between the factorization corrections on the visible cross sections measured using different luminometers. As an example, the results for the polynomial Gaussian model are shown using the data from the diagonal scan and the closest (third) vdM scan following it with the central values for the orbit drift (OD) corrected separations. Each subplot contains the measurements for all colliding bunch pairs with good fit results. The red lines show the diagonal with equal corrections to guide the eye. The uncertainties are statistical only. Strong correlations are visible as expected in the case of a stable shape model and well-understood luminometers. All of these measurements are used to define the final correction and its uncertainty, which is independent of the luminometer as it can only depend on the bunch shapes.

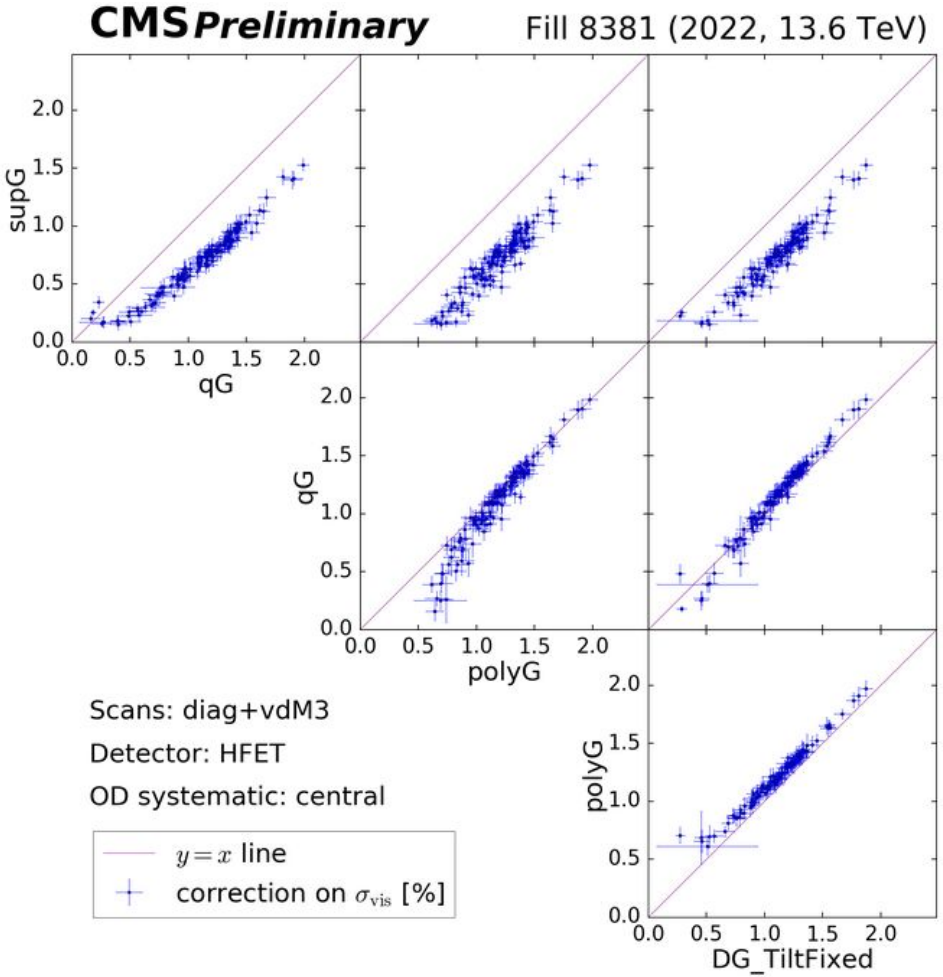

Corrections with Different 2D Models

Figure 11: Correlation between the factorization corrections on the visible cross section σ_{vis} measured using different 2D shape models. As an example, the results are shown for the HFET data from the diagonal scan and the closest vdM scan following it, with the central values for the orbit drift (OD) corrected separations. Each subplot contains the measurements for all colliding bunch pairs with good fit results. The red lines show the diagonal with equal corrections to guide the eye. The uncertainties are statistical only. Strong correlations are visible, with the super Gaussian model giving the smallest corrections. All of these measurements are used to define the final correction and its uncertainty, which should not dependent on the a priori 2D shape models, only on the bunch shapes.

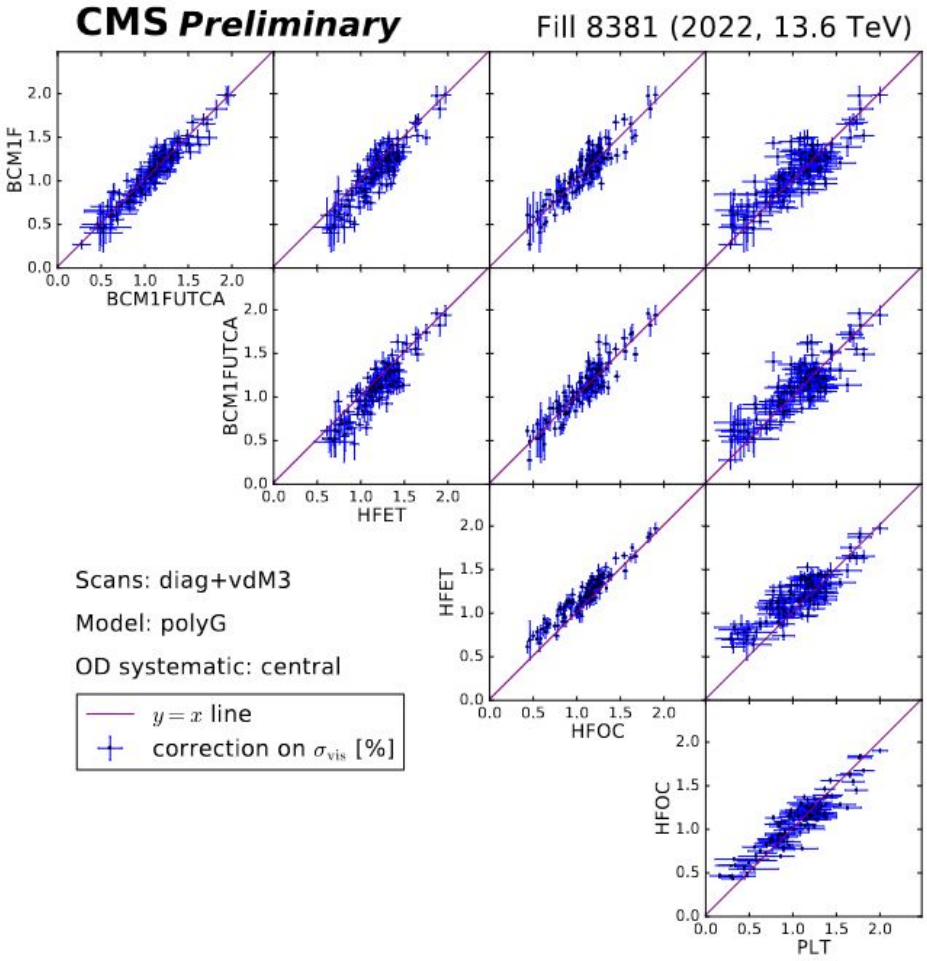

Correction vs 2D shape model

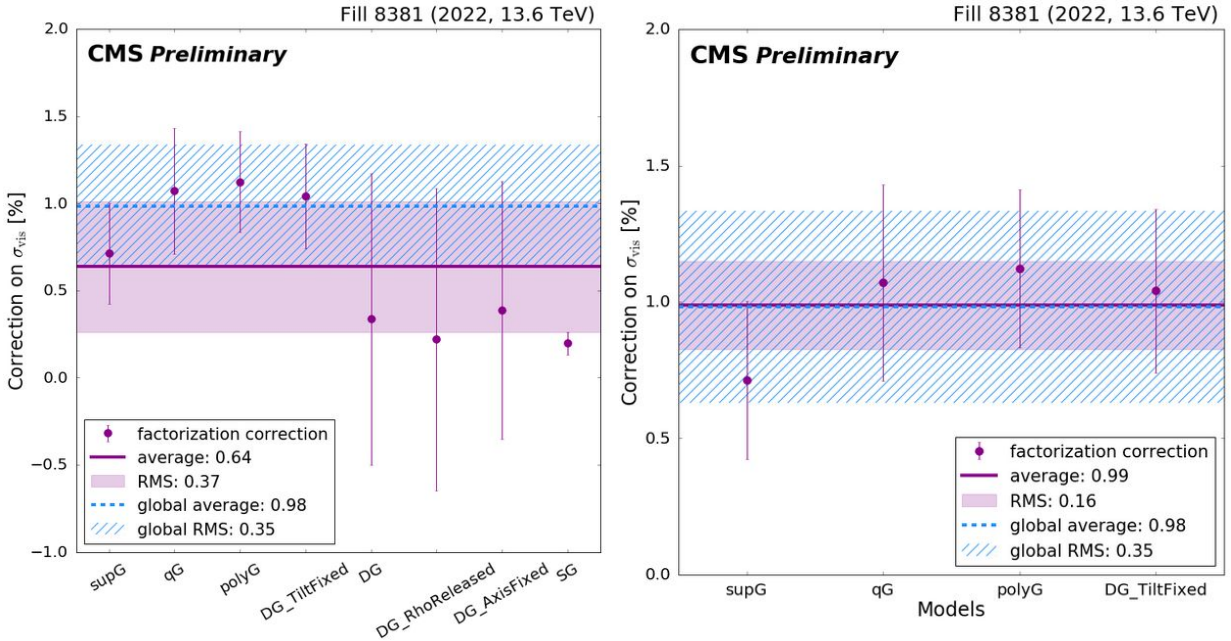

Figure 12: Factorization corrections on the visible cross section σ_{vis} for the various 2D models tested: (left) all models, (right) zoomed to only the stable non-trivial models that are used for the central value of the final correction (marked as “global average” with its RMS as uncertainty in the legend). An additional model systematics of 0.7% accounts for the results of the three unstable double Gaussian models. The single Gaussian model can not account for the dominant source of non-factorization and is not included in the global average. Each value is an average over the measurements performed by the 5 luminometers, using the data of 7 on-axis scan - off-axis scan pairs, and 144 colliding bunch pairs, with 9 orbit drift configurations. The average over the models with its RMS as uncertainty is given in the legend, together with the global average and its RMS over all more than 350k measurements. The right plot illustrates that the model dependence for the four stable 2D models has a sub-dominant contribution to the observed variations. The dominant uncertainty (0.7%) comes from the significantly lower corrections predicted by the less stable double Gaussian models.

Correction vs Time

Figure 13: Factorization corrections on the visible cross section σ_{vis} for the various on-axis scan - off-axis scan pairs arranged by the data taking time. Each value is an average over the measurements performed by the 5 luminometers on the data of 144 colliding bunch pairs using 9 orbit drift configurations, and 4 stable 2D shape models. The points from left to right correspond to vdM2+diag, diag+vdM3, vdM3+mini1, vdM3+offs, mini1+vdM4, offs+vdM4, vdM4+mini2 combinations. The average over the scan-scan combinations with its RMS as uncertainty is given in the legend, together with the global average and its RMS over all more than 350k measurements. This illustrates that the time dependence (if any) has a negligible contribution to the observed variations.

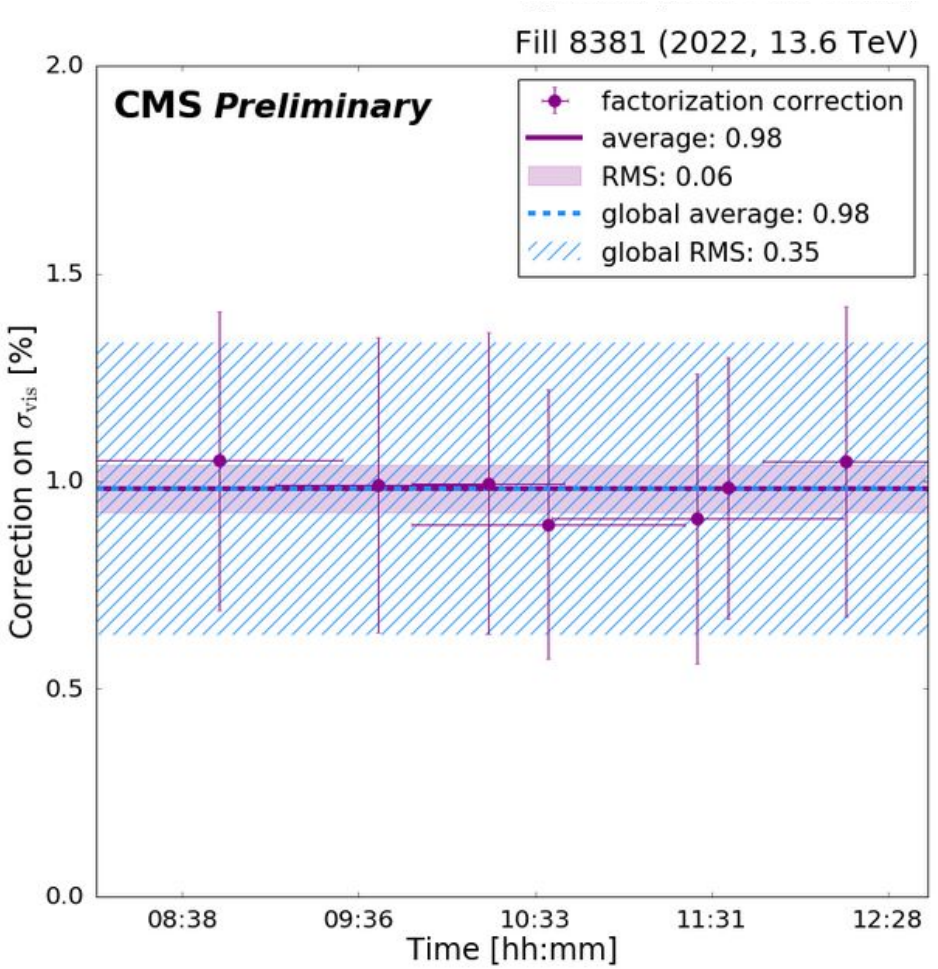

Correction vs BCID

Figure 14: Factorization corrections on the visible cross section σ_{vis} for the various bunch crossing identification (BCID) values arranged from 0 to 3563 along the LHC orbit. Each value is an average over the measurements performed by the 5 luminometers, using the data of 7 on-axis scan - off-axis scan pairs, with 9 orbit drift configurations, and 4 stable 2D shape models. The average over the BCIDs with its RMS as uncertainty is given in the legend, together with the global average and its RMS over all more than 350k measurements. This illustrates that the BCID dependence has a dominant contribution to the observed variations. The size of the correction correlates strongly with the collision pattern of the bunches (i.e. in which experiments the participating bunches collide) which is indicated by the color code just above the horizontal axis. For the notation, see the next slide. Every fourth BCID tend to have a lower correction, which could be related to the filling sequence which has a periodicity of 4 in the PS Booster.

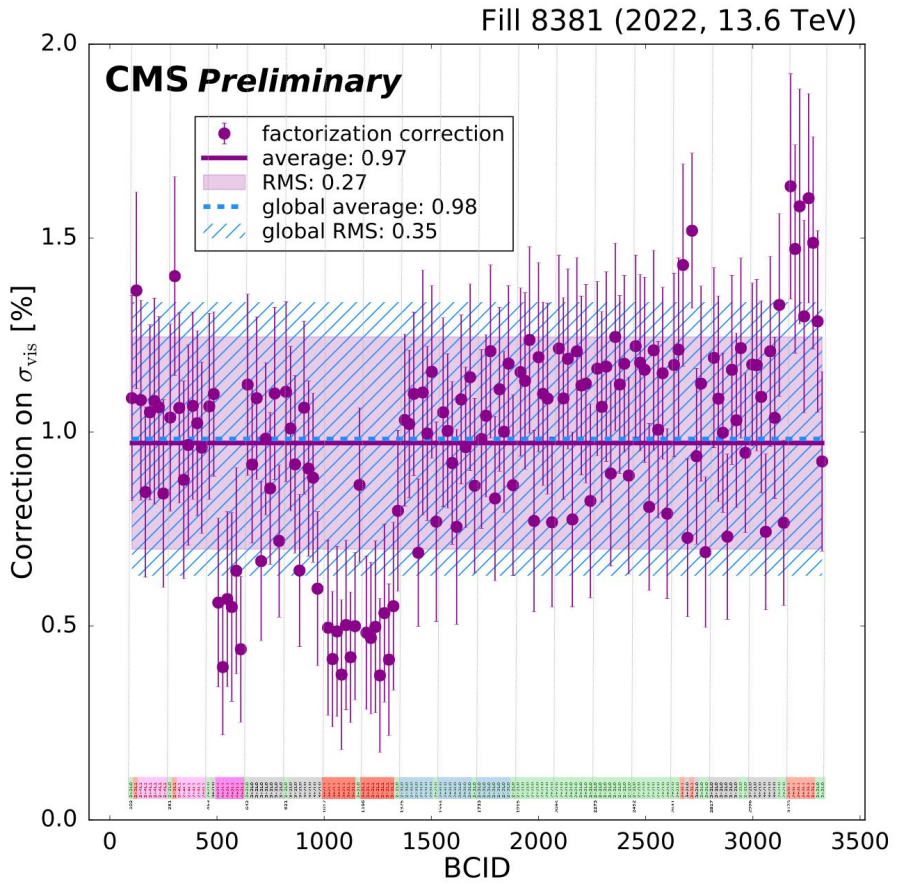

Bunch collision patterns in 2022 pp vdM fill 8381

Not a CMS plot, for illustration only

All bunches that collide at CMS (IP5) also collide at ATLAS (IP1) due to the symmetry of the accelerator.

Notation: n+mLx
n: number of IPs where the bunch in beam 1 collides (n>=2)
m: number of IPs where the bunch in beam 2 collides (n>=2)
x: number of collisions at IP8 (LHCb)

In more detail:
2+2L0: bunch in beam 1 and bunch beam 2 collides only at IP1 and IP5
3+2L0: bunch in beam 1 also collides at IP2 (ALICE)
3+2L1: bunch in beam 1 also collides at IP8 (LHCb)
2+3L0: bunch in beam 2 also collides at IP2 (ALICE)
2+3L1: bunch in beam 2 also collides at IP8 (LHCb)
4+2L1: bunch in beam 1 collides at all for IPs
2+4L1: bunch in beam 2 collides at all for IPs

LHC filling scheme: 525ns_146b_144_35_22_8bpi_20inj_noncloseLR.csv